Improved radiative corrections to (e, e′p) experiments: Explicit treatment of kinematical corrections in multiphoton bremsstrahlung

Florian Weissbach,[1,2] Kai Hencken,[2,3] Daniela Kiselev,[2,4] and Dirk Trautmann[2]

[1]*GSI Helmholtzzentrum für Schwerionenforschung mbH, D-64291 Darmstadt, Germany*
[2]*Departement für Physik, Universität Basel, CH-4056 Basel, Switzerland*
[3]*ABB Schweiz AG, Corporate Research, CH-5405 Baden-Dättwil, Switzerland*
[4]*Paul Scherrer Institut, CH-5232 Villigen, Switzerland*

Radiative processes lead to important corrections to (e, e′p) experiments. While radiative corrections can be calculated exactly in QED and to a good accuracy also including hadronic corrections, these corrections cannot be included into data analyses to arbitrary orders exactly. Nevertheless consideration of multiphoton bremsstrahlung above the low-energy cutoff is important for many (e, e′p) experiments. To date, higher-order bremsstrahlung effects concerning electron scattering experiments have been implemented approximately by employing the soft-photon approximation (SPA). In this paper we propose a novel approach to multiphoton emission which partially removes the SPA from (e, e′p) experiments. In this combined approach one hard photon is treated exactly; and additional (softer) bremsstrahlung photons are taken into account resorting to the soft-photon approximation. This partial removal of the soft-photon approximation is shown to be relevant for the missing-energy distribution for several kinematic settings at MAMI and TJNAF energies.

I. INTRODUCTION

Coincidence electron scattering experiments are an important tool for probing both nuclear structure and the structure of the nucleons. $A(e, e'p)(A-1)$ experiments (A being the atomic number) are, e.g., used to study the independent particle shell model and spectral functions and, in connection with that, occupation numbers and correlations. And the (e, e′p) reaction has also been employed to study the structure of, e.g., the proton electric form factor in the so-called Rosenbluth technique, apparently differing from polarization transfer measurements [1].

Results from electron scattering experiments are subject to radiative corrections, i.e., QED amplitudes going beyond the leading-order Born term (see Fig. 1). These corrections are of relative order α, but since they come with large logarithmic corrections they can contribute significantly to the cross section. Vertex correction, vacuum polarization, self-energy diagrams, and the two-photon exchange (TPE) are referred to as *internal radiative corrections*. And the four bremsstrahlung diagrams constitute the *external radiative corrections* and are the main focus of this paper. By introducing a small parameter associated with the photon energy resolution of the detectors, E_0, one can split up the cross section into a 'nonradiative part' including vertex corrections, vacuum polarization, self-energy contributions, TPE, and the emission of soft bremsstrahlung photons with energies below E_0; and into a 'radiative part', accounting for the emission of bremsstrahlung photons with energies above the low-energy cutoff E_0 [2]. The individual contributions from the internal and external radiative correction diagrams are divergent. It has first been shown by Schwinger [3] that by introducing the low-energy cutoff these divergences cancel.

The emission of bremsstrahlung alters the particle momenta and energies seen by the detectors and has to be corrected for in data analyses. Mo and Tsai first discussed this feature of electron scattering experiments [2,4], considering single-photon bremsstrahlung exactly, aside from an approximation in the calculation of the TPE contribution. Multiphoton emission is only included for soft photons with energies smaller than E_0. A comprehensive review on radiative corrections can be found in Ref. [5].

In order to obtain the desired experimental accuracy radiative corrections cannot be limited to the second order amplitudes. One has to take into account higher-order bremsstrahlung processes (multiphoton emission) above the low-energy cutoff [6–8] which is straightforward in soft-photon approximation (SPA). In SPA, multiphoton emission translates to a simple exponentiation of the bremsstrahlung contribution because of a factorization of the bremsstrahlung cross section [6–8]. A bremsstrahlung photon of energy ω^0 has no effect on the electron-proton scattering in the limit where $\omega^0 \to 0$. In this limit bremsstrahlung amplitudes factorize into the first-order Born amplitude times the amplitude for emitting a soft photon. The factorization also holds for multiphoton emission, if each emitted photon has vanishing energy. Summing over all orders of soft-photon emission then leads to exponentiation which also gives the cross section the correct asymptotic behavior as the parameter $E_0 \to 0$ [3,5,9]. Strictly speaking the SPA is only valid in the limit where all bremsstrahlung photon energies go to zero. In data analyses the approximation is applied however to emission of bremsstrahlung photons with finite energies [10]. The question arises up to which upper bound for the maximum bremsstrahlung photon energy the SPA is a good approximation.

While single-photon corrections to electron scattering experiments have been calculated exactly, including hadronic loops to a good accuracy [2,4,8] and including the proton
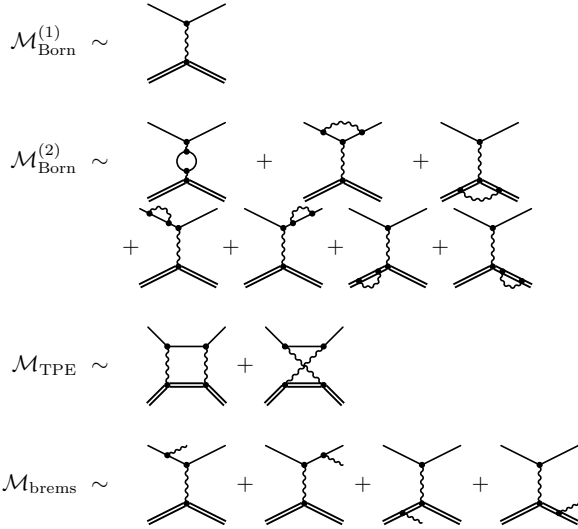
FIG. 1. Feynman diagrams beyond the leading order. The Feynman diagrams $\mathcal{M}_{\text{Born}}^{(1)}$ and $\mathcal{M}_{\text{Born}}^{(2)}$ constitute the Born approximation. $\mathcal{M}_{\text{TPE}}$ contains the two-photon exchange (TPE) diagrams. Together, the vacuum polarization, the vertex corrections, and the self-energy diagrams contained in $\mathcal{M}_{\text{Born}}^{(2)}$, and the two diagrams from $\mathcal{M}_{\text{TPE}}$ are referred to as internal radiative corrections. $\mathcal{M}_{\text{brems}}$ contains the external radiative corrections.

structure [11], multiphoton data analyses are usually performed in SPA. It allows both for straightforward inclusion of higher-order bremsstrahlung and for straightforward Monte Carlo generation of the bremsstrahlung photon angular distribution [10]. The purpose of this paper is to improve the multiphoton radiative correction treatment for $(e, e'p)$ experiments at MAMI and TJNAF energies by partially removing the SPA from multiphoton radiative corrections.

As the dominant contribution to bremsstrahlung in $(e, e'p)$ experiments comes from electron bremsstrahlung, we will initially omit bremsstrahlung originating from the proton. In Sec. IV we will then include proton bremsstrahlung with recourse to SPA, showing that proton bremsstrahlung is only a minor correction to the full radiative corrections.

The two TPE diagrams (see Fig. 1) go beyond the Born approximation and have received a lot of attention recently in H$(e, e'p)$ experiments studying the proton electric form factor [1,12,13]. Here we do not consider them further.

II. MULTIPHOTON SPA CROSS SECTION

The emission of a single photon by, e.g., the scattered electron (denoted here as "ef") is

$$\mathcal{M}_{\text{ef}} = ie^3 \bar{u}(k')\gamma^\alpha \varepsilon_\alpha \left[\frac{i\gamma^\nu (k' + \omega)_\nu + m}{(k' + \omega)^2 - m^2} \right] \gamma^\mu u(k)$$
$$\times \frac{1}{q^2} \bar{U}(p')\Gamma_\mu(q^2)U(p), \qquad (1)$$

where k and k' are the four-momenta of the incident and the scattered electron; and p and p' are the four-momenta of the incident and final proton. The electron and proton spinors are denoted by u and U, respectively. The momentum transfer to

the proton is defined by

$$q \equiv k - k' - \omega. \qquad (2)$$

Here $\omega = \omega^0(1, \Omega_\gamma)$ denotes the four-momentum of the bremsstrahlung photon and ε from Eq. (1) is its helicity. The vertex

$$\Gamma_\mu(q^2) \equiv F_1(q^2)\gamma_\mu + \frac{i\kappa F_2(q^2)}{4M}\sigma_{\mu\nu}q^\nu \qquad (3)$$

contains the electromagnetic structure of the target nucleus. M and m are the proton and electron masses, respectively. In the limit where the photon energy ω^0 vanishes the SPA can be applied and the single-photon emission amplitude (1) simplifies yielding [14,15]

$$\mathcal{M}_{\text{ef}} \sim e\mathcal{M}_{\text{Born}}^{(1)} \left(\frac{-k \cdot \varepsilon}{k \cdot \omega} \right). \qquad (4)$$

Here the first-order Born amplitude is given by

$$\mathcal{M}_{\text{Born}}^{(1)} = ie^2 \bar{u}(k')\gamma^\mu u(k)\frac{1}{q^2}\bar{U}(p')\Gamma_\mu U(p). \qquad (5)$$

The factorization of the SPA amplitude (4) also applies to the other three bremsstrahlung diagrams contained in $\mathcal{M}_{\text{brems}} = \mathcal{M}_{\text{ei}} + \mathcal{M}_{\text{ef}} + \mathcal{M}_{\text{pi}} + \mathcal{M}_{\text{pf}}$, the first letters of the subscripts referring to the particle emitting the bremsstrahlung photon (e for electron, p for proton), the second one indicating whether the photon was emitted before (i) or after (f) the scattering (see Fig. 1).

Summing and averaging over the spins and performing the QED traces, we obtain the factorized single-photon cross section as

$$\frac{d^5\sigma}{d\Omega_e d\Omega_\gamma d\omega^0} = \frac{d\sigma_{\text{Born}}^{(1)}}{d\Omega_e}\frac{A_{\text{el}}(\Omega_\gamma)}{\omega^0}, \qquad (6)$$

where $\frac{d\sigma^{(1)}}{d\Omega_e}$ is the elastic first-order electron-proton scattering Born cross section and

$$A_{\text{el}}(\Omega_\gamma) \equiv -\frac{\alpha(\omega^0)^2}{4\pi^2} \left(\frac{k'}{k' \cdot \omega} - \frac{k}{k \cdot \omega} + \frac{p}{p \cdot \omega} - \frac{p'}{p' \cdot \omega} \right)^2 \qquad (7)$$

is the SPA angular distributions of the bremsstrahlung photon [8]. The subscript 'el' indicates that the four-momenta are evaluated according to elastic kinematics.

This distribution (7) exhibits peaks as a function of the photon angles Ω_γ in the directions of the incident electron, the scattered electron, and the recoiling proton. Observing that most of the bremsstrahlung is emitted along the k-direction and the k'-direction, Schiff introduced the so-called peaking approximation for inclusive (e, e') experiments in 1952 [16] which was extended to exclusive $(e, e'p)$ experiments [8,17, 18], approximating the angular distribution (7) by

$$A_{\text{el}}(\Omega_\gamma) \sim \lambda_e \delta(\Omega_\gamma - \Omega_e) + \lambda_{e'}\delta(\Omega_\gamma - \Omega_{e'})$$
$$+ \lambda_{p'}\delta(\Omega_\gamma - \Omega_{p'}), \qquad (8)$$

and can be found, e.g., in Ref. [8]. The functions λ_e, $\lambda_{e'}$, and $\lambda_{p'}$ can be obtained by integrating the k-, k'-, and p'-contribution to the angular distribution (7). The peaking approximation can

be removed from $(e, e'p)$ data analyses, as has been shown in Ref. [10].

Now we consider the SPA cross section for multiphoton bremsstrahlung with total photon energy below the low-energy cutoff E_0 together with the emission of n photons with energies above the cutoff, which is given as [8]

$$
\begin{aligned}
\frac{d\sigma(n, E_0)}{d\Omega_e d\omega_1^0 d\Omega_{\gamma_1} \cdots d\omega_n^0 d\Omega_{\gamma_n}} &= \frac{d\sigma^{(1)}}{d\Omega_e} \exp[-\delta_{\text{soft}}(E_0)] \\
&\times (1 - \delta_{\text{hard}}) \\
&\times \frac{1}{n!} \frac{A_{\text{el}}(\Omega_{\gamma_1})}{\omega_1^0} \cdots \frac{A_{\text{el}}(\Omega_{\gamma_n})}{\omega_n^0} \\
&\times \theta(\omega_1^0 - E_0) \cdots \theta(\omega_n^0 - E_0).
\end{aligned}
\tag{9}
$$

As mentioned above the exponential function accounts for multiphoton emission below the cut-off energy E_0 to all orders. $\delta_{\text{soft}}(E_0)$ contains the bremsstrahlung contributions (see $\mathcal{M}_{\text{brems}}$ in Fig. 1). And δ_{hard} comprises contributions from the vertex corrections, vacuum polarization, and self-energy diagrams. The full definitions for these two terms can be found in Ref. [8]. The integration techniques necessary to derive Eq. (9) are given, e.g., in Ref. [19].

We sum the cross section (9) over all n photons and we integrate over the photon energies up to an upper limit E_{tot}, which is a parameter associated with the cuts applied to the data. We also introduce an acceptance function χ_A^n. This acceptance function allows to get not only the total, but also the differential cross section, or ones where the detection of some of the particles is only in some kinematical range, by selections different functions for χ_A^n. We obtain then the photon-integrated cross section [10] as

$$
\begin{aligned}
\frac{d\sigma}{d\Omega_e}[\chi_A] &= \frac{d\sigma^{(1)}}{d\Omega_e} \exp[-\delta_{\text{soft}}(E_0)](1 - \delta_{\text{hard}}) \\
&\times \sum_{n=0}^{\infty} \frac{1}{n!} \left[\lambda \log\left(\frac{E_{\text{tot}}}{E_0}\right) \right]^n \\
&\times \left[\prod_{i=1}^{n} \int_{E_0}^{E_{\text{tot}}} \frac{d\omega_i^0 d\Omega_\gamma}{\lambda \omega_i^0 \log\left(\frac{E_{\text{tot}}}{E_0}\right)} \chi_A^n \right].
\end{aligned}
\tag{10}
$$

Here χ_A^n is a function of the electron and photon kinematic variables (for photons with energies larger than E_0), $\chi_A^n = \chi_A^n(\Omega_e, \omega_1^0, \Omega_1, \ldots, \omega_n^0, \Omega_n)$, which is the probability for an event to be seen in $\frac{d\sigma}{d\Omega_e}[\chi_A]$ [10]. In Eq. (10) E_{tot} is chosen such that all bremsstrahlung photons with nonvanishing χ_A^n are included in the integration, and λ is the integral of $A(\Omega_\gamma)$ over the angular distribution, see Eq. (7),

$$
\lambda \equiv \int d\Omega_\gamma A_{\text{el}}(\Omega_\gamma).
\tag{11}
$$

The cross section (10) is independent of the cutoff E_0 in the limit where E_0 becomes small (see, e.g., Ref. [8]).

Because the bremsstrahlung photons are usually not measured in electron scattering experiments[1] they need to be integrated out. This can efficiently be done by a Monte Carlo integration. This is the basis of a Monte Carlo event generator, where individual 'events,' i.e., values for all kinematical variables, are generated together with a weight, such that their distribution corresponds to the differential cross section. Once the radiative corrections have been simulated the experimental data can be corrected for the radiative effects.

The cross section (10) is therefore written in terms of a probability density function for the variables $\Omega_{\gamma i}$ and ω_i and is then used to generate bremsstrahlung events with certain photon energies, multiplicities, and angular distributions in a Monte Carlo event generator [10]. The Monte Carlo algorithm assigns a weight to each event. By summing over these weights for each observable needed and choosing the χ_A^n as bins in these observables we get the differential cross sections shown later.

The Monte Carlo routine we introduce in this paper generates multiple photons according to the cross section (10). The photon multiplicities n follow a Poisson distribution and the bremsstrahlung energies are essentially distributed according to $1/\omega_i^0$ [10]. The bremsstrahlung photon angles are generated according to the elastic angular distribution $A_{\text{el}}(\Omega_\gamma^i)$ from Eq. (7), using the elastic $(e, e'p)$ kinematics for the electron and proton momenta, by a rejection algorithm. The index i indicates that each individual photon from a multiphoton event follows the angular distribution (7).

The SPA simplifies multiphoton bremsstrahlung calculations considerably by the factorization of the cross section. $(e, e'p)$ data analysis procedures additionally adjust the kinematics of the $(e, e'p)$ reaction. The form factors are evaluated at an adjusted value of q^2 [8,17,18], following a suggestion by Borie and Drechsel [20,21], rendering the treatment of radiative corrections more systematic. We refer to this extended version of the SPA as the 'modified SPA', or mSPA, which accounts for the bremsstrahlung photons' effect on the electron-proton scattering process approximately via a modification of the kinematics only.

III. MULTIPHOTON BREMSSTRAHLUNG EVENT GENERATION BEYOND SPA

One way to extend the SPA for single-photon bremsstrahlung is to calculate the cross section not in elastic kinematics but in the real 1γ-kinematic settings: Given the photon's four-momentum and the beam energy and fixing, e.g., the electron scattering angles, one calculates the remaining kinematic quantities. The cross section is then calculated using the new 1γ-kinematic variables, additionally inserting the correct value of q^2 with one photon emitted into the form factors.

Data analyses cannot include an exact multiphoton QED treatment, since the exact multiphoton amplitudes cannot be included into the calculations to arbitrarily high orders.

---

[1]Because of the essential $1/\omega^0$ energy dependance most bremsstrahlung photons emitted have very small energies such that they cannot be measured.

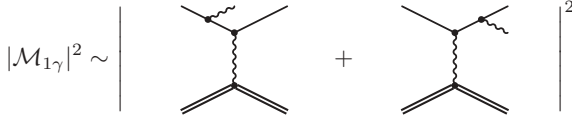$$|\mathcal{M}_{1\gamma}|^2 \sim \left| \quad + \quad \right|^2$$

FIG. 2. The 1γ matrix element $\mathcal{M}_{1\gamma} = \mathcal{M}_{\text{ei}} + \mathcal{M}_{\text{ef}}$ squared.

Therefore we suggest a new *combined approach*: we generate multiphoton bremsstrahlung according to the SPA distribution. We choose one hard photon from each scattering event which we treat exactly by calculating the exact QED 1γ matrix element for electron bremsstrahlung (see Fig. 2) from $\mathcal{M}_{1\gamma} = \mathcal{M}_{\text{ei}} + \mathcal{M}_{\text{ef}}$. We then treat the remaining photons as soft photons (with energies still larger than the low-energy cutoff E_0), employing the SPA.

There are several possibilities to choose the hard photon. We have implemented and compared the following four:

(i) The photon with the largest energy ω^0 is chosen as the hard photon. This method addresses the question of the validity of the SPA. In this approach the choice for the hard photon depends on the choice of the reference frame, in contrast to the other approaches described here.

(ii) Calculating the momentum transfer squared, $q_{1\gamma}^2 = k - k' - \omega$, for each photon of the multiphoton event we choose the photon yielding a value of $q_{1\gamma}^2$ which deviates most from the elastic value, q_{el}^2.

(iii) Calculating the momentum transfer squared in multiphoton kinematics, q_{tot}^2 (where $q_{\text{tot}} = k - k' - \sum_i \omega_i$), the photon is chosen which leads to a value of $q_{1\gamma}^2$ which is closest to q_{tot}^2. This method and method 2 focus on both the kinematic aspects of bremsstrahlung emission and on the appropriate calculation of the form factors.

(iv) Choose the 'hard' photon randomly. This approach was tested in order to demonstrate the influence of the hard photons on the result.

These approaches have been implemented by reweighting our SPA Monte Carlo generator described above, by the ratio of the matrix element of the improved approach and the SPA matrix element.

To make the notation less cluttered, we absorb the photon energy dependence into the angular distribution $A(\Omega_\gamma^i)$,

$$a(\omega_i) \equiv \frac{A(\Omega_i)}{\omega_i^0}. \tag{12}$$

In SPA the 1γ-bremsstrahlung matrix element squared for the hard photon (see Fig. 2) then reads

$$\left|\mathcal{M}_{1\gamma}^{\text{SPA}}\right|^2 \approx \left|\mathcal{M}_{\text{Born}}^{(1)}\right|^2 a_{\text{el}}(\omega). \tag{13}$$

In order to distinguish mSPA calculations (where the kinematic setting are adjusted in order to account for the bremsstrahlung photon's effect on the hard scattering process) from the elastic calculation of the same amplitude we add the subscripts 'mSPA' and 'el', respectively, to the angular distribution (12) in the remainder of this paper.

Considering single-photon bremsstrahlung first, we assign to each bremsstrahlung event generated by the Monte Carlo algorithm a weight which is then used in the binning in order to obtain differential and total cross section. First we define the 'exact 1γ weight' by

$$w_{1\gamma}^{\text{ex}} \equiv \frac{|\mathcal{M}_{1\gamma}|^2}{\left|\mathcal{M}_{\text{Born}}^{(1)}\right|^2 a_{\text{el}}(\omega)}. \tag{14}$$

This weight divides out the approximate SPA matrix element and replaces it by the exact matrix element for single-photon radiation. In contrast to the exact weight (14), the mSPA weight measures the influence of the mSPA,

$$w_{1\gamma}^{\text{mSPA}} \equiv \frac{\left|\mathcal{M}_{\text{Born}}^{(1)\text{mSPA}}\right|^2 a_{\text{mSPA}}(\omega)}{\left|\mathcal{M}_{\text{Born}}^{(1)}\right|^2 a_{\text{el}}(\omega)}, \tag{15}$$

where $\mathcal{M}_{\text{Born}}^{(1)\text{mSPA}}$ is the first-order Born amplitude $\mathcal{M}_{\text{Born}}^{(1)}$ evaluated in mSPA kinematics. As the exact weight (14) the mSPA weight (15) reweights the event, but now for the case of the SPA matrix elements in modified kinematics replacing $q = k - k'$ by $\tilde{q} = k - k' - \omega$. So the first-order Born amplitude $\mathcal{M}_{\text{Born}}^{(1)\text{mSPA}}$ as well as the photon distribution $a_{\text{mSPA}}(\omega)$ in the *numerator* are evaluated in 1γ-kinematics (or mSPA kinematics which is the same in this case).

This approach can be extended to multiphoton bremsstrahlung. Assuming that the n bremsstrahlung photons have been ordered such that the nth photon is the hard photon, we define the "combined $n\gamma$" weight as

$$w_{n\gamma}^{\text{comb}} \equiv \frac{|\mathcal{M}_{1\gamma}(\omega_{\text{hard}})|^2 a_{\text{mSPA}}(\omega_1) \cdots a_{\text{mSPA}}(\omega_{n-1})}{\left|\mathcal{M}_{\text{Born}}^{(1)}\right|^2 a_{\text{el}}(\omega_{\text{hard}}) a_{\text{el}}(\omega_1) \cdots a_{\text{el}}(\omega_{n-1})}, \tag{16}$$

where a_{mSPA} is the angular photon distribution in modified SPA; and we define the modified weight as

$$w_{n\gamma}^{\text{mSPA}} \equiv \frac{\left|\mathcal{M}_{\text{Born}}^{(1)\text{mSPA}}\right|^2}{\left|\mathcal{M}_{\text{Born}}^{(1)}\right|^2}$$

$$\times \frac{a_{\text{mSPA}}(\omega_{\text{hard}}) a_{\text{mSPA}}(\omega_1) \cdots a_{\text{mSPA}}(\omega_{n-1})}{a_{\text{el}}(\omega_{\text{hard}}) a_{\text{el}}(\omega_1) \cdots a_{\text{el}}(\omega_{n-1})}, \tag{17}$$

where $\mathcal{M}_{\text{Born}}^{(1)\text{mSPA}}$ is the first-order Born amplitude evaluated in mSPA.

The Monte Carlo routine introduced here generates multiphoton events in SPA. Each scattering event is assigned two weights (16) and (17) using the four methods for selecting the hard photon, described at the beginning of this section. In order to check the combined approach against data (where available) and against SPA simulations, we embedded the combined Monte Carlo routine into SIMC, a Monte Carlo simulation for electron scattering experiments from TJNAF [17]. This data analysis code uses a version of the mSPA which does not choose a hard photon from a given multiphoton bremsstrahlung event, but treats all photons in SPA. In addition it uses the peaking approximation [16,17]. Thus we were able to compare the error associated with the use of the SPA with other sources of errors.

In order to additionally include the effect of proton bremsstrahlung in the combined approach, we inserted it, assuming the mSPA is a good approximation for proton

bremsstrahlung, the overall effect of proton bremsstrahlung being small anyway. The first-order electron bremsstrahlung is still calculated exactly. This was achieved by modifying the weight (16) into

$$w_{n\gamma}^{comb} \equiv \left[|\mathcal{M}_{1\gamma}(\omega_{hard})|^2 + \left|\mathcal{M}_{Born}^{(1)}\right|^2 a_{rest}(\omega_{hard}) \right]$$

$$\times \frac{a_{mSPA}(\omega_1) \cdots a_{mSPA}(\omega_{n-1})}{\left|\mathcal{M}_{Born}^{(1)}\right|^2 a_{el}(\omega_{hard}) a_{el}(\omega_1) \cdots a_{el}(\omega_{n-1})}, \quad (18)$$

where $a_{rest}(\omega_{hard})$ is the angular distribution (7) without the electron-electron terms. [In addition (7) has been divided by ω_{hard}^0.] We generated the photon angular distribution using this approach, comparing it to the combined calculation without the proton (16).

IV. RESULTS

To test the combined calculation we simulated the missing-energy distributions and the photon angular distributions at several kinematic settings. 10^7 events per run were generated in order to get good statistics for the different yields. The results turned out to be indistinguishable under approaches 1, 2, and 3 for choosing the hard photon (see previous section). Only the random choice of the hard photon (approach 4) deviated from the other methods. The results presented in this section are therefore based on approach 1, which is simple to implement and to use.

Figures 3 and 4 show multiphoton missing-energy distributions, once calculated in mSPA (17), once calculated using the combined approach (16) for two kinematic settings. We see that the mSPA calculations overestimate the radiative tails. While the deviations between the two calculations are of the order of a few percent for missing energies below $E_m = 100 \, \text{MeV}$, the deviations become considerably larger toward the far ends of the radiative tails.
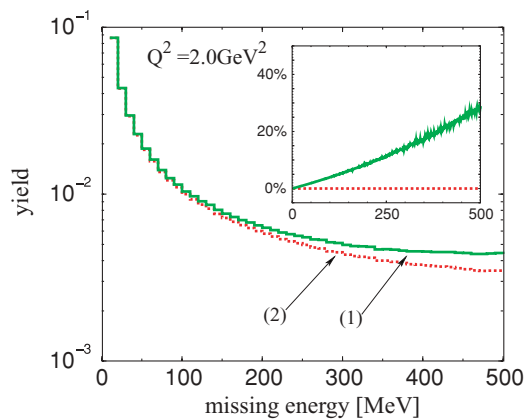
FIG. 3. (Color online) Missing energy distribution for multi-photon bremsstrahlung. The solid curve (1) (green) was obtained using the modified SPA weight (17). The dotted curve (2) (red) represents the combined approach using weight (16). The inset graph shows the deviation between the two curves in percent, normalized to the combined result. At $E_m = 100 \, \text{MeV}$ the modified SPA calculation overestimates the radiative tail by 3.9%, at $E_m = 500 \, \text{MeV}$ the deviation is 29%. The momentum transfer is $Q^2 = 2.0 \, \text{GeV}^2$.
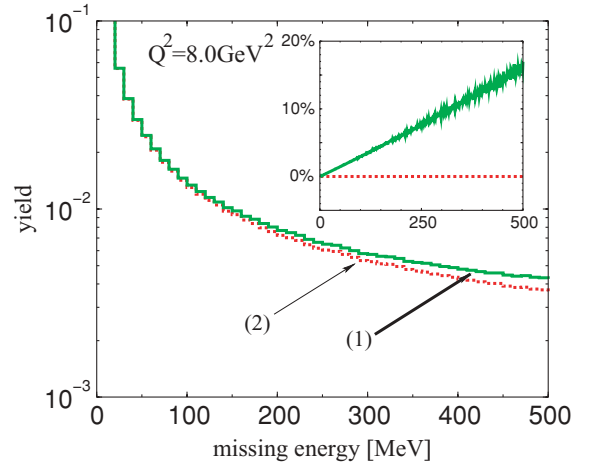
FIG. 4. (Color online) Missing-energy distribution for multiphoton bremsstrahlung. The attribution of the curves is as above in Fig. 3. At $E_m = 100 \, \text{MeV}$ the modified SPA calculation overestimates the radiative tail by 3.0%, at $E_m = 500 \, \text{MeV}$ the deviation is 17%. The momentum transfer is $Q^2 = 8.0 \, \text{GeV}^2$.

Since we want to evaluate the importance of the SPA in multiphoton radiative corrections it is important to compare the effect of the improved radiative corrections to other sources of errors, present in $(e, e'p)$ experiments. On top of radiative corrections, $(e, e'p)$ experiments are, e.g., corrected for finite detector resolution, for particle decays, and for multiple scattering [17,18].

The simulations shown in Figs. 5 and 6 take into account radiative corrections, detector resolution, particle decays, and multiple scattering. They indicate that the combined approach has an impact on the missing-energy distribution which is not dominated by the other corrections. The radiative tails calculated following the combined approach are stronger than the radiative tails obtained with the standard SIMC radiative correction procedure for all kinematic settings considered.
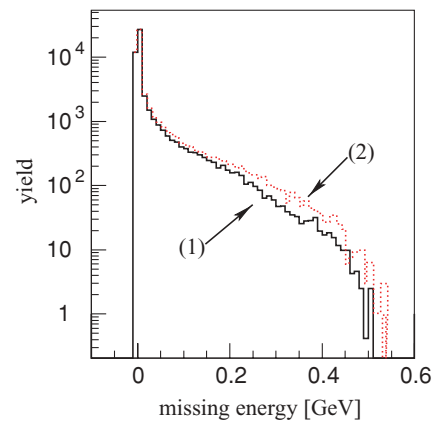
FIG. 5. (Color online) Missing-energy distribution for multiphoton bremsstrahlung simulated with SIMC. The solid curve (1) (black) represents the standard SIMC modified SPA radiative corrections. The dotted curve (2) (red) shows the E_m distribution obtained by inserting our combined radiative correction approach into SIMC. The latter one has more strength in the radiative tail. The total yield differs by 2.3%. The momentum transfer is $Q^2 = 2.0 \, \text{GeV}^2$, as in Fig. 3.
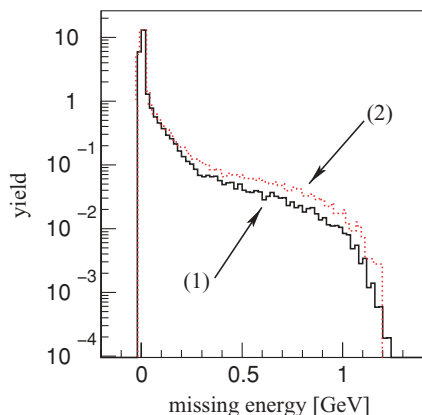
FIG. 6. (Color online) Missing-energy distribution for multiphoton bremsstrahlung simulated with SIMC. The attribution of the curves is the same as in Fig. 5. The total yield differs by 1.4%. The momentum transfer is $Q^2 = 8.0 \, \text{GeV}^2$, as in Fig. 4.

As a second observable we considered the angular distribution of the bremsstrahlung photons. As for the missing-energy distributions we first looked at radiative corrections only. Then we additionally took into account other corrections. The photon angular distributions are shown in Figs. 7 and 8. For all kinematic settings the mSPA calculations overestimate the angular distribution in the vicinity of the incident electron, that is, at small angles. As for the missing energy the question is whether this deviation can be seen in the data, or whether other sources of errors dominate the photon angular distribution. In order to determine the impact of the combined approach on the photon angular distribution we resort again to SIMC, as in the case of the missing-energy distribution.

Using standard SIMC for comparison implies that the peaking approximation is employed [17]. It is clear that the photon angular distribution, generated in SIMC's standard radiative correction approach differs from the combined approach even more than the mSPA from the combined calculation shown in Figs. 7 and 8 (see also Ref. [10]). The peaking approximation
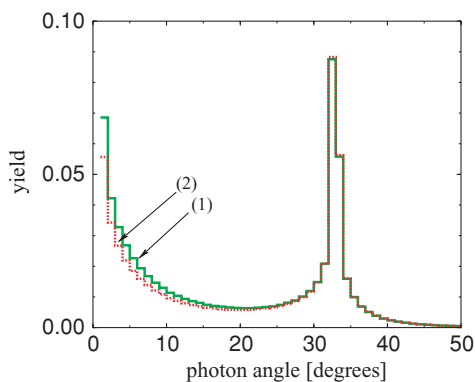

FIG. 7. (Color online) Angular bremsstrahlung photon distribution. The solid curve (1) (green) represents the modified SPA, the dotted curve (2) (red) shows the combined approach. The SPA distribution deviates from the combined calculation especially in the vicinity of the incident electron, around $0°$. The kinematic settings are as in Fig. 3.
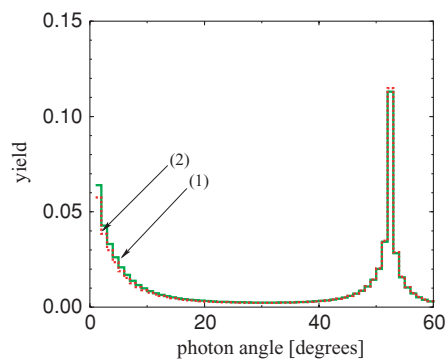

FIG. 8. (Color online) Angular bremsstrahlung photon distribution. The attribution of the curves is as in Fig. 7. The SPA distribution deviates from the combined calculation especially in the vicinity of the incident electron, around $0°$. The kinematic settings are as in Fig. 4.

and thus the standard SIMC analysis code is known not to describe the experimental angular distribution accurately in between the two radiation peaks coming from the incident and the scattered electron [10]. Nevertheless, looking at the photon angular distributions both with the standard SIMC code and with the modified version of SIMC, containing our combined simulation, gives us the opportunity to rate the impact of our approach compared to the standard SIMC radiative correction procedure. Where available, we compared the different approaches to data.

Figures 9 and 10 show the photon angular distributions as generated by SIMC in comparison to our combined approach. The largest deviations between the two appear in the middle between the peaks due to e and e' bremsstrahlung. This is in
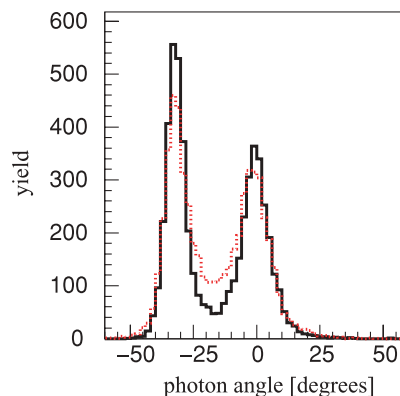

FIG. 9. (Color online) Angular bremsstrahlung photon distribution generated with SIMC. The solid curve (1) (black) represents the standard SIMC modified SPA calculation. The dotted curve (2) (red) shows the angular distribution simulated with the combined approach. The largest difference between the standard SIMC treatment and the data occurs in the middle between the e and e' directions and in the height of the two peaks. This is due to the peaking approximation which is used by the standard SIMC code; it overestimates the peaks. The comparison with experimental data can be found in Fig. 11. The kinematics are the same as in Figs. 3 and 7.
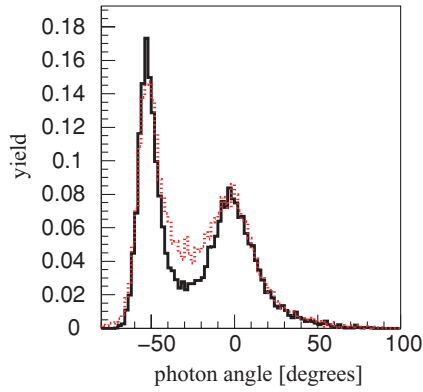
FIG. 10. (Color online) Angular bremsstrahlung photon distribution generated with SIMC. The attribution of the curves is the same as in Fig. 9 but there was no data available for these kinematic settings. They are the same as in Figs. 4 and 8.

contrast to Figs. 7 and 8 where deviations occur at small angles. This indicates that the small deviations between SPA and combined approach seen at small angles (see Figs. 7 and 8) are washed out by other effects. The photon angular distribution is not affected by the SPA and by the combined approach. The dominant approximation is the peaking approximation here.

Figure 11 shows experimental data for the photon angular distribution reconstructed from the H($e, e'p$) scattering (TJNAF experiment E97-006, [22,23]) and verifies this conclusion. This measurement at $Q^2 = 2.0\,\text{GeV}^2$ shows that both the mSPA calculation and the combined approach describe the data well.

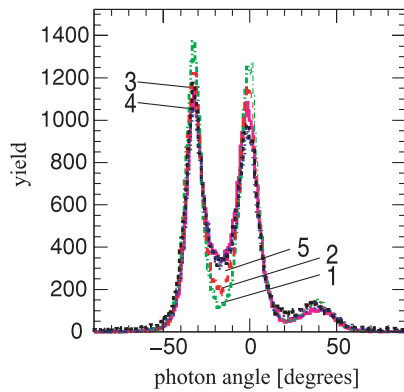As can be seen in Fig. 12, including mSPA proton bremsstrahlung does not change the photon angular distri-

FIG. 11. (Color online) Angular bremsstrahlung photon distribution for H($e, e'p$) scattering generated with SIMC and compared to data. The bump on the right hand side at the proton direction is an artefact due to protons punching through the spectrometers. The dash-dotted curve (1) (green) and the (2) (red) curve show standard SIMC photon distributions, both using different versions of the peaking approximation. The dotted curve (3) (black) represents the data. The solid line (4) (magenta) is the new combined approach implemented into SIMC. Additionally there is a blue line (5) from Ref. [10] showing a full angular SPA simulation. The kinematics are the same as in Figs. 3 and 7. The combined approach (4) fits the data well.
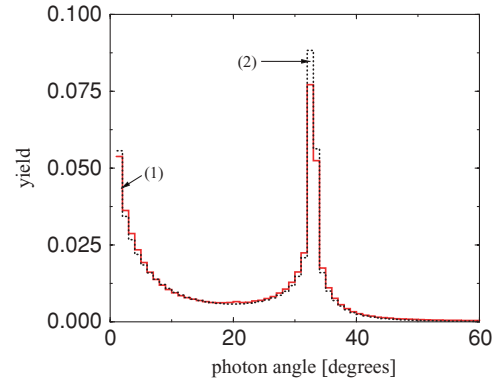

FIG. 12. (Color online) Photon angular distribution with (1) (solid curve, red) and without (2) (dotted curve, black) SPA proton bremsstrahlung. The simulation neglecting proton bremsstrahlung overestimates the electron peaks slightly. In the rest of the photon angle domain the two curves coincide. The momentum transfer $Q^2 = 2.0\,\text{GeV}^2$.

bution considerably. Neglecting the proton bremsstrahlung just leads to a slight overestimation of the peaks due to electron bremsstrahlung. The missing energy is not changed at all by including proton bremsstrahlung (see Fig. 13). We conclude that the proton bremsstrahlung does not influence the results significantly and therefore mSPA can be used safely.

We observe that in the case considered here the combined approach reproduces the experimental photon angular distribution much better than the standard SIMC simulation using the peaking approximation. The combined approach presented in this manuscript and the full angular approach from Ref. [10] are much closer to each other and to the data than the standard SIMC simulations, indicating, again, that removal of the peaking approximation is more important for the photon angular distribution than the partial removal of the SPA, as presented here.
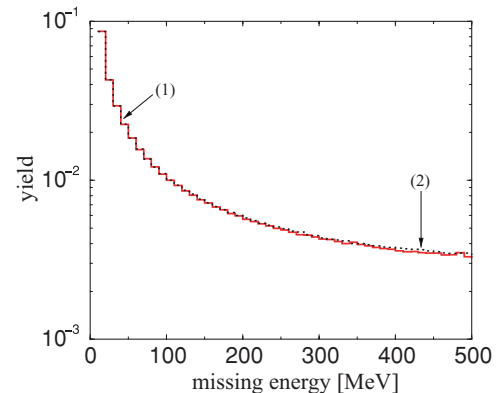

FIG. 13. (Color online) Missing energy with (1) (solid curve, red) and without (2) (dotted curve, black) SPA proton bremsstrahlung. The two curves are hardly distinguishable. The momentum transfer $Q^2 = 2.0\,\text{GeV}^2$.

V. DISCUSSION AND CONCLUSION

We have shown that it is feasible to improve $(e, e'p)$ radiative corrections by partially removing the SPA from multiphoton bremsstrahlung processes. Our results are invariant under three different approaches to choosing the hard photon whereas a random choice of the hard photon is neither consistent with the other three approaches nor with a comparison to data. Treating one photon as a hard photon improves the kinematic treatment of the $(e, e'p)$ reaction.

We compare the combined approach to multiphoton mSPA calculations, looking at the missing-energy distribution. The mSPA overestimates the radiative tail for different kinematic settings. In order to check whether the combined treatment has an influence when considering additional experimental corrections we subsequently inserted our combined calculation into an existing data analysis code, which in its standard version is using the peaking approximation and a version of mSPA, in addition to other corrections [8,17]. We showed that that our combined approach has an impact on the missing-energy distribution and that it was not hidden by other sources

of background and other effects like, e.g., detector resolution. The computational expense of the combined method was small, at most a factor of 2, compared to a standard data analysis code.

Similarly, we showed that the photon angular distribution was overestimated by mSPA especially at small angles, in the vicinity of the incident electron. Inserting our combined approach into SIMC we saw large deviations between the standard SIMC photon angular distribution and our combined approach. The bulk of this difference was due to the peaking approximation, as has already been suggested in Ref. [10]. The photon angular distribution is hardly sensitive to deviations originating from mSPA.

Our combined approach takes radiative corrections for $(e, e'p)$ experiments beyond both the peaking approximation and the soft-photon approximation. And it treats both the kinematic impact of multiphoton bremsstrahlung and the evaluation of the form factors at modified momentum transfers more systematically than previous $(e, e'p)$ radiative correction procedures. We have also shown that the SPA can safely be used for proton bremsstrahlung.

[1] J. Arrington, Phys. Rev. C **68**, 034325 (2003).

[2] L. W. Mo and Y. S. Tsai, Rev. Mod. Phys. **41**, 205 (1969).

[3] J. Schwinger, Phys. Rev. **75**, 898 (1949).

[4] Y. S. Tsai, Phys. Rev. **122**, 1898 (1961).

[5] L. C. Maximon, Rev. Mod. Phys. **41**, 193 (1969).

[6] D. R. Yennie, S. C. Frautschi, and H. Tsuura, Ann. Phys. (NY) **13**, 379 (1961).

[7] S. N. Gupta, Phys. Rev. **99**, 1015 (1955).

[8] R. Ent, B. W. Filippone, N. C. R. Makins, R. G. Milner, T. G. ONeill, and D. A. Wasson, Phys. Rev. C **64**, 054610 (2001).

[9] F. Bloch and A. Nordsieck, Phys. Rev. **52**, 54 (1937).

[10] F. Weissbach *et al.*, Eur. Phys. J. A **30**, 477 (2006).

[11] L. C. Maximon and J. A. Tjon, Phys. Rev. C **62**, 054320 (2000).

[12] P. G. Blunden, W. Melnitchouk, and J. A. Tjon, Phys. Rev. Lett. **91**, 142304 (2003).

[13] P. A. M. Guichon and M. Vanderhaeghen, Phys. Rev. Lett. **91**, 142303 (2003).

[14] L. D. Landau and E. M. Lifshitz, *Quantum Electrodynamics*, 2nd ed. (Pergamon, Oxford, 1982), p. 431.

[15] S. Weinberg, *The Quantum Theory of Fields* (Cambridge University Press, Cambridge, England, 1995), Vol. 1.

[16] L. I. Schiff, Phys. Rev. **87**, 750 (1952).

[17] J. Arrington, SIMC 2001 release, TJNAF.

[18] P. E. Ulmer, MCEEP, release 3.8, TJNAF.

[19] G. 't Hooft, Nucl. Phys. **B61**, 455 (1973).

[20] E. Borie and D. Drechsel, Nucl. Phys. **A167**, 369 (1971).

[21] E. Borie, Z. f. Naturforschung **30a**, 1543 (1975).

[22] D. Rohe *et al.* (E97-006 Collaboration), Phys. Rev. Lett. **93**, 182501 (2004).

[23] D. Rohe *et al.*, Eur. Phys. J. A **17**, 439 (2003).